Available online at www.sciencedirect.com
ScienceDirect
Ocean Engineering 34 (2007) 2231–2239
OCEAN ENGINEERING
www.elsevier.com/locate/oceaneng

Hydrodynamic shape optimization of thin floating plates

Christopher J. Damaren*

University of Toronto, Institute for Aerospace Studies, 4925 Dufferin Street, Toronto, Ont., Canada M3H 5T6

Received 22 March 2007; accepted 19 June 2007
Available online 5 July 2007

Abstract

In this work, the problem of optimizing the shape of a thin floating plate (sometimes called a dock) to maximize radiation damping is investigated. The plate is modeled with zero draft and floats on the surface of an irrotational, incompressible ocean of infinite extent. For simplicity, only rigid heave motions are considered. The flow problem is analyzed using the Chen and Mei variational principle wherein the potential field inside a hemisphere surrounding the plate is represented using a spherical harmonic expansion and matched on the hemisphere to an outer field described by distributing sources on the hemisphere. The plate shape is parameterized using a Fourier series which is suitable for use with the variational principle. Gradients of the damping coefficient with respect to the shape parameters are developed by solving an adjoint flow problem whose potential is shown to be a scalar multiple of the original flow potential. Optimal plate shapes are determined using the well-known optimization code NPSOL which makes use of the damping coefficient calculation and gradients.

Keywords: Hydrodynamic shape optimization; Free-surface hydrodynamics; Floating plates

1. Introduction

Many engineering problems are characterized by structures interacting with a surrounding fluid. Examples are aircraft and ships. Efficient operation of these structures requires an appropriate degree of shape optimization. This has reached a high degree of maturity in the problem of airfoil shape optimization; see for example (Nemec et al., 2004). The optimization of floating structures has been less studied but there has been some work by Clauss and Birk (1996) and Ragab (2001, 2004).

Recently, there has been considerable research into very large floating structures (VLFS) with some focus on floating airports. Proposed and current structures are characterized by small draft compared to the horizontal dimensions of the mat-like structure. Hence, it is defensible to model them as thin plate structures. The large dimensions make them considerably flexible and this mandates hydroelastic analyses. Recent work in this area is summarized in the survey of Watanabe et al. (2004). An analysis of floating circular plates has been done by Andrianov and Hermans (2005), while Damaren (2001) has studied the rectangular case.

Suppression of the vertical motions of these structures requires appropriate sources of energy dissipation. These include structural damping (including both material effects and those due to articulations such as joints), viscous fluid effects, and radiation damping due to the production of outgoing surface waves. It is the last of these that concerns us here and we desire to optimize the planform shape of a thin floating plate to maximize the radiation damping effect. It is expected that radiation damping will dominate over the other two effects in applications. The analysis of Yeung (1982) for the transient analysis of a floating circular cylinder is consistent with this. That included only wave effects and the prediction for the free decay of the motion of a circular cylinder exhibited excellent agreement with experiment. The damping ratio of the free decay (approximately 0.18) is considerably larger than that expected from structural damping alone. In the present work, for simplicity, we only consider rigid-body heave motion. Since this does not involve flexible deformation of the plate, structural damping can be neglected.

*Tel.: +1 416 667 7704; fax: +1 416 667 7799.
E-mail address: damaren@utias.utoronto.ca

0029-8018/$ - see front matter © 2007 Elsevier Ltd. All rights reserved.
doi:10.1016/j.oceaneng.2007.06.005

The plate is assumed to float on the free surface of an inviscid, incompressible, and irrotational ocean of infinite depth. The objective is to maximize the radiation damping in heave for a given prescribed area with constraints on the perimeter and minimum dimensions. The boundary of the plate is parameterized using a Fourier series as a function of angular position in the free surface.

The potential flow problem is solved using the variational principle developed by Chen and Mei (1974) and detailed by Mei (1989). The inner field within a hemisphere encompassing the plate is described using a spherical harmonic expansion which ideally suits the geometry given the zero-draft nature of the plate. It also allows integrals involving the shape of the plate to be performed accurately and derivatives involving the shape to be carried out analytically. The outer field is described by distributing sources on the exterior of the hemisphere and it along with its normal derivative is matched to those of the inner field using the variational principle. This methodology was previously used by Damaren (2001) to study rectangular plates of fixed dimension.

The shape optimization is carried out using the general purpose optimization code NPSOL (Gill et al., 1998) which is based on a sequential quadratic programming algorithm. The code requires the specification of the objective function, constraints, and gradients. Although gradients of the objective function can be determined using finite difference calculations, this requires multiple evaluations of the objective function and is prone to subtractive cancelation errors in evaluating the differences. This is particularly problematic since free-surface hydrodynamic calculations are usually only accurate to a few significant figures.

In this paper we apply the adjoint approach to determining the gradients. This was pioneered by Jameson (1988) in aerodynamic shape optimization and has more recently been applied to shape optimization of surface vessels by Ragab (2001, 2004). In the latter works, the objective was to minimize the wave resistance at forward speed. However, a potential flow formulation was used. Our approach has a similar methodology but is made specific to the time-harmonic treatment of a floating body. In particular, the gradient of the damping coefficient with respect to the shape parameters is determined. This is greatly simplified by the fact that the adjoint potential flow solution is shown to be a scalar multiple of that of the original flow problem.

2. Hydrodynamic boundary value problem

Consider the vertical motion of a thin floating plate lying in the free surface of an irrotational, incompressible ocean of infinite depth. We use a coordinate system $\mathbf{r} = [x \;\; y \;\; z]^{\mathrm{T}}$ where the plane $z = 0$ corresponds to the mean free surface and the z-axis is vertically upward. The origin corresponds to the geometric center of the plate which we also assume is the mass center given a homogeneous mass distribution. The wetted surface of the plate is denoted by $\mathsf{B}(\mathbf{a})$ where $\mathbf{a}$ denotes the shape parameters which uniquely define B. The undisturbed free surface is designated as $\mathsf{F}(\mathbf{a})$ which is the surface $z = 0$ less the plate surface B. The undisturbed fluid occupies V which is the half-space $z \leqslant 0$ less the plate surface B. It is assumed to be bounded by a cylinder S_∞ whose radius tends to infinity and whose bottom B_∞ tends towards infinite depth (see Fig. 1).

The vertical motion of the plate in heave is given by $w(x, y, t)$ and we consider a single mode with time-harmonic motion:

$$w(x, y, t) = \mathrm{Re}\{q_\alpha w_\alpha(x, y) \mathrm{e}^{\mathrm{j}\omega t}\}, \tag{1}$$

where $w_\alpha \equiv 1$ (rigid body heave mode) but we explicitly exhibit it in the development so as to indicate the procedure for general motions. The motion equation assuming a rigid plate is given by

$$\sigma \ddot{w}(x, y, t) = p(x, y, t), \tag{2}$$

where σ is the constant mass density per unit area and $p(x, y, t)$ is the hydrodynamic pressure.

The motion of the fluid is governed by the velocity potential $\Phi(\mathbf{r}, t)$ which in V satisfies Laplace's equation $\nabla^2 \Phi = 0$. It can be written as

$$\Phi(\mathbf{r}, t) = \mathrm{Re}\{\mathrm{j}\omega q_\alpha \mathrm{e}^{\mathrm{j}\omega t} \phi_\alpha(\mathbf{r})\}, \tag{3}$$

where the spatial function $\phi(\mathbf{r}) = \phi_\alpha(\mathbf{r})$ satisfies the following equations:

$$\nabla^2 \phi = 0 \quad \text{in } \mathsf{V}, \tag{4}$$

$$\mathscr{B}(\phi) = \frac{\partial \phi}{\partial z} - w_\alpha = 0 \quad \text{on } \mathsf{B}(\mathbf{a}), \tag{5}$$

$$\mathscr{M}(\phi) = \frac{\partial \phi}{\partial z} - k\phi = 0 \quad \text{on } \mathsf{F}(\mathbf{a}), \tag{6}$$

$$\mathscr{A}(\phi) = \frac{\partial \phi}{\partial z} = 0 \quad \text{on } \mathsf{B}_\infty, \tag{7}$$

$$\mathscr{T}(\phi) = \frac{\partial \phi}{\partial r} + \mathrm{j}k\phi = 0 \quad \text{on } \mathsf{S}_\infty, \tag{8}$$

where $k = \omega^2/g$ and g is the acceleration due to gravity. The last of these is recognized as the radiation condition where $r = \sqrt{x^2 + y^2}$.

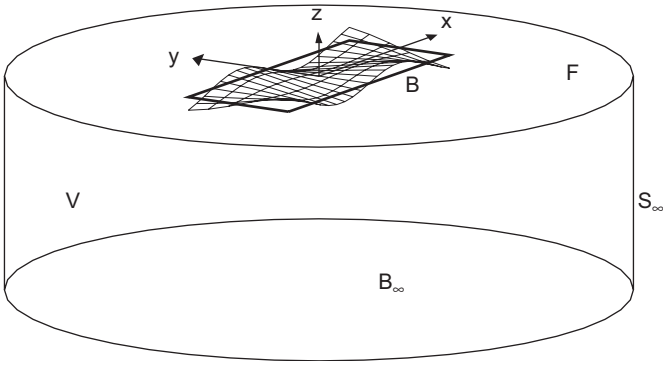

Fig. 1. Fluid domain with floating plate.

Using Bernoulli's equation the linearized fluid pressure is given by

$$p(x,y,t) = -\rho \frac{\partial \Phi}{\partial t} - \rho g z.$$

When this is substituted into the motion equation in Eq. (2), we arrive at

$$-\omega^2 m_\alpha \,\mathrm{Re}\{q_\alpha e^{j\omega t}\} = \mathrm{Re}\{f_\alpha e^{j\omega t}\},$$

where $m_\alpha = \int_{\mathsf{B}} \sigma w_\alpha^2 \,\mathrm{d}S$. The (generalized) force coefficient is given by

$$f_\alpha = -j\omega H_{\alpha\alpha} q_\alpha - K_{\alpha\alpha} q_\alpha, \tag{9}$$

where $K_{\alpha\alpha} = \rho g \int_{\mathsf{B}} w_\alpha^2 \,\mathrm{d}S$ is the hydrostatic restoring force stiffness and the radiation impedance is

$$H_{\alpha\alpha} = j\omega\rho \int_{\mathsf{B}} \phi w_\alpha \,\mathrm{d}S = j\omega\mu_{\alpha\alpha} + \lambda_{\alpha\alpha} \tag{10}$$

with

$$\lambda_{\alpha\alpha} = -\omega\rho \int_{\mathsf{B}} w_\alpha \,\mathrm{Im}\,\phi \,\mathrm{d}S,$$

$$\mu_{\alpha\alpha} = \rho \int_{\mathsf{B}} w_\alpha \,\mathrm{Re}\,\phi \,\mathrm{d}S.$$

Here, $\lambda_{\alpha\alpha}$ is the damping coefficient and $\mu_{\alpha\alpha}$ is the added mass coefficient. It is well known that the damping coefficient is associated with the production of outgoing wave radiation and the degree of energy dissipation for the body is proportional to it (Mei, 1989). Hence, our objective is to determine the shape of plate $\mathbf{a}$ which maximizes $\lambda_{\alpha\alpha}$ and we write the objective function as

$$\mathscr{J}(\mathbf{a}) = \lambda_{\alpha\alpha} = \int_{\mathsf{B}(\mathbf{a})} \mathscr{F}(\phi) \,\mathrm{d}S, \quad \mathscr{F}(\phi) = -\omega\rho w_\alpha \,\mathrm{Im}\,\phi. \tag{11}$$

The evaluation of $\mathscr{J}(\mathbf{a})$ is described in Section 3 and the determination of the gradient $\mathrm{d}\mathscr{J}/\mathrm{d}\mathbf{a}$ is developed in Section 4.

3. Variational formulation of the radiation problem

We now develop a solution for the flow problem, i.e., given $\mathbf{a}$ evaluate $\mathscr{J}$. A classic formulation of the problem distributes sources on the plate but it has been shown that this approach breaks down when the floating body lies in the free surface (Damaren, 2001). Here we use the methodology proposed there, wherein the solution in an inner region containing the plate is matched to an outer solution which satisfies the radiation condition (see Fig. 2). Let S denote the surface of a hemisphere of radius a_h which encloses the plate and is centered at the origin. (The selection of a_h will be discussed in Section 5.) Let $\widetilde{\mathsf{V}}$ denote the interior of S and $\bar{\mathsf{V}}$ denote its complement in V, i.e., $\bar{\mathsf{V}} \cup \widetilde{\mathsf{V}} = \mathsf{V}$. Let $\widetilde{\mathsf{F}}$ denote the circular free surface in S less the plate surface B. The free surface corresponding to $\bar{\mathsf{V}}$ is denoted by $\bar{\mathsf{F}}$. Hence, $\bar{\mathsf{F}} \cup \widetilde{\mathsf{F}} = \mathsf{F}$.

For the radiation problem, we seek a solution $\phi = \widetilde{\phi}$ in $\widetilde{\mathsf{V}}$ which satisfies Eqs. (4)–(6). In the exterior region, we desire

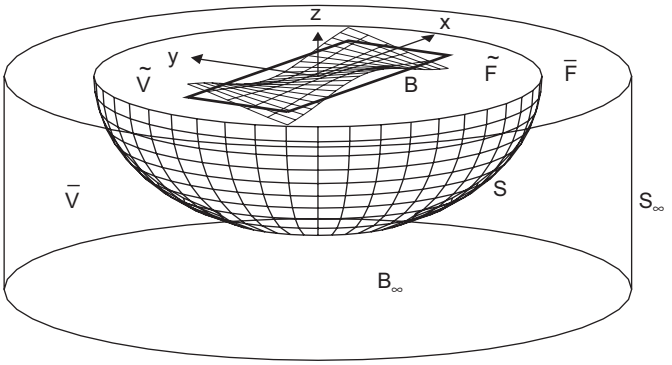

Fig. 2. Discretization for variational formulation.

a solution $\phi = \bar{\phi}$ which satisfies Laplace's equation, the free surface condition on $\bar{\mathsf{F}}$, the bottom condition in Eq. (7), and the radiation condition in Eq. (8). In addition, the two solutions should be matched on S:

$$\widetilde{\phi}(\mathbf{r}) = \bar{\phi}(\mathbf{r}), \quad \frac{\partial \widetilde{\phi}}{\partial n}(\mathbf{r}) = \frac{\partial \bar{\phi}}{\partial n}(\mathbf{r}), \quad \mathbf{r} \in \mathsf{S}, \tag{12}$$

where n is the outward normal to the hemisphere.

The variational principle of Chen and Mei (1974) as detailed by Mei (1989) provides a solution to the problem. Here, one minimizes the functional

$$\mathscr{K}(\widetilde{\phi}, \bar{\phi}) = \frac{1}{2}\int_{\widetilde{\mathsf{V}}} \nabla\widetilde{\phi} \cdot \nabla\widetilde{\phi} \,\mathrm{d}V - \frac{1}{2}k \int_{\widetilde{\mathsf{F}}} \widetilde{\phi}^2 \,\mathrm{d}S - \int_{\mathsf{B}} \widetilde{\phi} w_\alpha \,\mathrm{d}A + \int_{\mathsf{S}} \left(\frac{1}{2}\bar{\phi} - \widetilde{\phi}\right) \frac{\partial \bar{\phi}}{\partial n} \,\mathrm{d}S. \tag{13}$$

This yields a function $\widetilde{\phi}$ which weakly satisfies Eq. (4) with Eqs. (5) and (6), and the matching conditions in Eq. (12) satisfied as natural boundary conditions. It is assumed that $\bar{\phi}$ is selected to exactly satisfy Eqs. (4) and (6)–(8).

Since $\widetilde{\phi}$ is bounded in $\widetilde{\mathsf{V}}$, including at the origin, it is proposed that it be expanded in spherical harmonics as

$$\widetilde{\phi}(\mathbf{r}) = \sum_{m=0}^{M_s} \sum_{n=m}^{N_s} A_{nm} \phi_{nm}(\mathbf{r}) + \sum_{m=1}^{M_s} \sum_{n=m}^{N_s} B_{nm} \psi_{nm}(\mathbf{r}), \tag{14}$$

where

$$\phi_{nm}(\mathbf{r}) = \left(\frac{R}{a_h}\right)^n P_n^m(\cos\theta) \cos m\chi,$$

$$\psi_{nm}(\mathbf{r}) = \left(\frac{R}{a_h}\right)^n P_n^m(\cos\theta) \sin m\chi.$$

The spherical coordinates $\{R, \theta, \chi\}$ are chosen such that

$$x = R\sin\theta\cos\chi, \quad y = R\sin\theta\sin\chi, \quad z = -R\cos\theta$$

and P_n^m are the associated Legendre functions as defined by Hulme (1982). On the free surface, $R = r = \sqrt{x^2 + y^2}$.

For the potential exterior to the hemisphere, we express $\bar{\phi}$ using a source distribution on S:

$$\bar{\phi}(\mathbf{r}) = \int_{\mathsf{S}} G(\mathbf{r}, \boldsymbol{\xi}) \gamma(\boldsymbol{\xi}) \,\mathrm{d}S_\xi, \tag{15}$$

where the source distribution $\gamma(\mathbf{r})$ is selected according to

$$\frac{\partial\bar{\phi}(\mathbf{r})}{\partial n} = -2\pi\gamma(\mathbf{r}) + \int_{\mathsf{S}} \frac{\partial G(\mathbf{r},\boldsymbol{\xi})}{\partial n_r}\gamma(\boldsymbol{\xi})\,\mathrm{d}S_\xi. \tag{16}$$

In practice, S is divided into a number of region S_i and $\gamma(\mathbf{r})$ is taken to be constant on each S_i with $\gamma_i = \gamma(\mathbf{r}_i)$ where $\mathbf{r}_i$ is the centerpoint of S_i. The Green's function $G(\mathbf{r},\boldsymbol{\xi})$ satisfies Laplace's equation (except at $\mathbf{r} = \boldsymbol{\xi}$), the free surface, bottom, and radiation conditions:

$$\begin{aligned} G(\mathbf{r},\boldsymbol{\xi}) = {} & \frac{1}{R_\xi} + \frac{1}{R_1} - k\mathrm{e}^{-Y}\left[\pi(Y_0(X) + \mathbf{H}_0(X)) \right.\\ & \left. + 2\int_0^Y \mathrm{e}^t(X^2+t^2)^{-1/2}\,\mathrm{d}t\right]\\ & - 2\pi\mathrm{j}k\mathrm{e}^{-Y}J_0(X) + \Delta G(\mathbf{r},\boldsymbol{\xi}), \end{aligned}$$

where

$$\begin{aligned} & r_\xi = \sqrt{(x-\xi)^2 + (y-\eta)^2},\\ & R_\xi = \sqrt{r_\xi^2 + (z-\zeta)^2}, \quad R_1 = \sqrt{r_\xi^2 + (z+\zeta)^2},\\ & X = kr_\xi, \quad Y = -k(z+\zeta). \end{aligned}$$

$J_0(X)$ and $Y_0(X)$ are the Bessel functions of the first and second kind, and $\mathbf{H}_0(X)$ is the Struve function. In this work, $G(\mathbf{r},\boldsymbol{\xi})$ and its normal derivative are calculated using the algorithms of Newman (1984). The perturbation $\Delta G(\mathbf{r},\boldsymbol{\xi})$ contains an additional source, dipoles, and wave-free potentials which prevent the occurrence of irregular frequencies. These terms are described in more detail by Damaren (2001) and the approach is based on the work by Ursell (1981).

The resulting potential and its normal derivative are taken to be piecewise constant on S with $\bar{\boldsymbol{\Phi}} = \mathrm{col}\{\bar{\phi}(\mathbf{r}_i)\}$ and $\bar{\boldsymbol{\Phi}}_n = \mathrm{col}\{\partial\bar{\phi}(\mathbf{r}_i)/\partial n\}$. Defining $\boldsymbol{\Gamma} = \mathrm{col}\{\gamma_i\}$, Eqs. (15) and (16) can be approximated by

$$\boldsymbol{\Phi} = \mathbf{G}\boldsymbol{\Gamma}, \quad \boldsymbol{\Phi}_n = \mathbf{H}\boldsymbol{\Gamma},$$

where

$$G_{ij} = G(\mathbf{r}_i,\mathbf{r}_j)\Delta S_j, \quad \Delta S_i = \int_{\mathsf{S}_i}\mathrm{d}S, \tag{17}$$

$$H_{ij} = -2\pi\delta_{ij} + \frac{\partial G(\mathbf{r}_i,\mathbf{r}_j)}{\partial n_r}\Delta S_j. \tag{18}$$

Substituting Eqs. (14)–(16) into the functional in Eq. (13) leads to

$$\mathscr{K}(\mathbf{b}) = \tfrac{1}{2}\mathbf{b}^{\mathrm{T}}\mathbf{W}\mathbf{b} - \mathbf{b}^{\mathrm{T}}\mathbf{c}, \tag{19}$$

where the interior and exterior fields are completely determined by

$$\mathbf{b} = \begin{bmatrix}\mathbf{A}\\ \boldsymbol{\Gamma}\end{bmatrix}, \quad \mathbf{A} = \begin{bmatrix}\mathrm{col}\{A_{nm}\}\\ \mathrm{col}\{B_{nm}\}\end{bmatrix}, \quad \mathbf{c} = \begin{bmatrix}\mathbf{g}\\ \mathbf{0}\end{bmatrix},$$
$$\mathbf{g} = \begin{bmatrix}\mathrm{col}\{g_{nm}\}\\ \mathrm{col}\{h_{nm}\}\end{bmatrix} \tag{20}$$

with

$$\begin{Bmatrix} g_{nm}\\ h_{nm}\end{Bmatrix} = P_n^m(0)\int_{\mathsf{B}}(r/a_h)^n\begin{Bmatrix}\cos m\chi\\ \sin m\chi\end{Bmatrix}w_\alpha\,\mathrm{d}S.$$

The assembling of the matrix $\mathbf{W} = \mathbf{W}^{\mathrm{T}}$ is detailed by Damaren (2001). Minimizing $\mathscr{K}$ in Eq. (19) with respect to $\mathbf{b}$ leads to the linear system of equations $\mathbf{W}\mathbf{b} = \mathbf{c}$. Substituting the spherical harmonic expansion in Eq. (14) into (11) yields the following expression for the damping coefficient:

$$\mathscr{J} = -\omega\rho\,\mathbf{g}^{\mathrm{T}}\,\mathrm{Im}\,\mathbf{A}, \tag{21}$$

where both $\mathbf{g}$ and $\mathbf{A}$ depend on the shape parameters $\mathbf{a}$ which are defined in the next section.

4. Adjoint formulation for shape optimization

The surface B will be written as $\mathsf{B}(\mathbf{a})$ where $\mathbf{a}$ are the shape parameters. Its boundary is described using polar coordinates as

$$r(\mathbf{a},\chi) = \frac{a_0}{2} + \sum_{n=1}^{N} a_n\cos n\chi, \tag{22}$$

where $\mathbf{a} = [a_0 \;\; a_1 \;\; \cdots \;\; a_N]^{\mathrm{T}}$.

The methodology developed by Ragab (2001, 2004) for free-surface potential flows will now be used to construct an adjoint problem which furnishes the gradients of the cost functional with respect to the shape parameters. Adjoining the constraints in Eqs. (4)–(8) to the cost functional in Eq. (11) using Lagrange multipliers yields

$$\begin{aligned} \mathscr{L}(\phi,\mathbf{a}) = {} & \int_{\mathsf{B}(\mathbf{a})}\mathscr{F}(\phi)\,\mathrm{d}S + \int_{\mathsf{V}}\psi\nabla^2\phi\,\mathrm{d}V + \int_{\mathsf{B}(\mathbf{a})}\beta\mathscr{B}(\phi)\,\mathrm{d}S\\ & + \int_{\mathsf{F}(\mathbf{a})}\mu\mathscr{M}(\phi)\,\mathrm{d}S + \int_{\mathsf{B}_\infty}\alpha\mathscr{A}(\phi)\,\mathrm{d}S\\ & + \int_{\mathsf{S}_\infty}\tau\mathscr{T}(\phi)\,\mathrm{d}S. \end{aligned}$$

Taking the first variation of this functional yields

$$\begin{aligned} \delta\mathscr{L} = {} & \delta\int_{\mathsf{B}(\mathbf{a})}\mathscr{F}(\phi)\,\mathrm{d}S + \int_{\mathsf{V}}\psi\nabla^2\delta\phi\,\mathrm{d}V + \delta\int_{\mathsf{B}(\mathbf{a})}\beta\mathscr{B}(\phi)\,\mathrm{d}S\\ & + \delta\int_{\mathsf{F}(\mathbf{a})}\mu\mathscr{M}(\phi)\,\mathrm{d}S + \int_{\mathsf{B}_\infty}\alpha\delta\mathscr{A}(\phi)\,\mathrm{d}S\\ & + \int_{\mathsf{S}_\infty}\tau\delta\mathscr{T}(\phi)\,\mathrm{d}S\\ = {} & \frac{\partial}{\partial\mathbf{a}}\left[\int_{\mathsf{B}(\mathbf{a})}(\mathscr{F}(\phi) + \beta\mathscr{B}(\phi))\,\mathrm{d}S + \int_{\mathsf{C}}\mu\mathscr{M}(\phi)\,\mathrm{d}S\right.\\ & \left. - \int_{\mathsf{B}(\mathbf{a})}\mu\mathscr{M}(\phi)\,\mathrm{d}S\right]\delta\mathbf{a}\\ & + \int_{\mathsf{B}(\mathbf{a})}\frac{\partial\mathscr{F}}{\partial\phi}\delta\phi\,\mathrm{d}S + \int_{\mathsf{V}}\psi\nabla^2\delta\phi\,\mathrm{d}V + \int_{\mathsf{B}(\mathbf{a})}\beta\frac{\partial\mathscr{B}}{\partial\phi}\delta\phi\,\mathrm{d}S \end{aligned}$$

$$+\int_{\mathsf{F}(\mathbf{a})}\mu\frac{\partial\mathscr{M}}{\partial\phi}\delta\phi\,\mathrm{d}S+\int_{\mathsf{B}_\infty}\alpha\frac{\partial\mathscr{A}}{\partial\phi}\delta\phi\,\mathrm{d}S+\int_{\mathsf{S}_\infty}\tau\frac{\partial\mathscr{T}}{\partial\phi}\delta\phi\,\mathrm{d}S. \tag{23}$$

Here, we have introduced C as the circular region consisting of $\mathsf{F}\cup\mathsf{B}$. Note that it does not depend on the shape parameters $\mathbf{a}$ and hence

$$\frac{\partial}{\partial\mathbf{a}}\int_{\mathsf{C}}\mu\mathscr{M}(\phi)\,\mathrm{d}S=\mathbf{0}$$

in Eq. (23).

Applying Green's second identity, we have

$$\begin{aligned}\int_{\mathsf{V}}(\psi\nabla^2\delta\phi-\delta\phi\nabla^2\psi)\,\mathrm{d}V=&\int_{\mathsf{B}(\mathbf{a})}\left(\psi\frac{\partial\delta\phi}{\partial z}-\delta\phi\frac{\partial\psi}{\partial z}\right)\mathrm{d}S\\&+\int_{\mathsf{F}(\mathbf{a})}\left(\psi\frac{\partial\delta\phi}{\partial z}-\delta\phi\frac{\partial\psi}{\partial z}\right)\mathrm{d}S\\&+\int_{\mathsf{B}_\infty}\left(-\psi\frac{\partial\delta\phi}{\partial z}+\delta\phi\frac{\partial\psi}{\partial z}\right)\mathrm{d}S\\&+\int_{\mathsf{S}_\infty}\left(\psi\frac{\partial\delta\phi}{\partial r}-\delta\phi\frac{\partial\psi}{\partial r}\right)\mathrm{d}S.\end{aligned}$$

Incorporating this into Eq. (23) while using the definitions in Eqs. (5)–(8) gives

$$\begin{aligned}\delta\mathscr{L}=&\frac{\partial}{\partial\mathbf{a}}\left\{\int_{\mathsf{B}(\mathbf{a})}[\mathscr{F}(\phi)+\beta\mathscr{B}(\phi)-\mu\mathscr{M}(\phi)]\,\mathrm{d}S\right\}\delta\mathbf{a}\\&+\int_{\mathsf{V}}\delta\phi\nabla^2\psi\,\mathrm{d}V+\int_{\mathsf{B}(\mathbf{a})}\frac{\partial\mathscr{F}}{\partial\phi}\delta\phi\,\mathrm{d}S\\&+\int_{\mathsf{B}(\mathbf{a})}\left[\psi\frac{\partial\delta\phi}{\partial z}-\delta\phi\frac{\partial\psi}{\partial z}+\beta\frac{\partial\delta\phi}{\partial z}\right]\mathrm{d}S\\&+\int_{\mathsf{F}(\mathbf{a})}\left[\psi\frac{\partial\delta\phi}{\partial z}-\delta\phi\frac{\partial\psi}{\partial z}+\mu\left(\frac{\partial\delta\phi}{\partial z}-k\delta\phi\right)\right]\mathrm{d}S\\&+\int_{\mathsf{B}_\infty}\left[-\psi\frac{\partial\delta\phi}{\partial z}+\delta\phi\frac{\partial\psi}{\partial z}+\alpha\frac{\partial\delta\phi}{\partial z}\right]\mathrm{d}S\\&+\int_{\mathsf{S}_\infty}\left[\psi\frac{\partial\delta\phi}{\partial r}-\delta\phi\frac{\partial\psi}{\partial r}+\tau\left(\frac{\partial\delta\phi}{\partial r}+\mathrm{j}k\delta\phi\right)\right]\mathrm{d}S.\end{aligned}$$

The adjoint problem for the Lagrange multipliers is determined by selecting them to suppress the integrals involving $\delta\phi$ and its normal derivatives. This yields

$$\nabla^2\psi=0\quad\text{in }\mathsf{V}, \tag{24}$$

$$\beta=-\psi,\quad\frac{\partial\psi}{\partial z}=\frac{\partial\mathscr{F}}{\partial\phi}\quad\text{on }\mathsf{B}(\mathbf{a}), \tag{25}$$

$$\mu=-\psi,\quad\frac{\partial\psi}{\partial z}=k\psi\quad\text{on }\mathsf{F}(\mathbf{a}), \tag{26}$$

$$\alpha=\psi,\quad\frac{\partial\psi}{\partial z}=0\quad\text{on }\mathsf{B}_\infty, \tag{27}$$

$$\tau=-\psi,\quad\frac{\partial\psi}{\partial r}+\mathrm{j}k\psi=0\quad\text{on }\mathsf{S}_\infty. \tag{28}$$

Comparing Eqs. (24)–(28) with Eqs. (4)–(8) shows that the boundary value problem for the adjoint case is identical with the original flow problem with the exception of the boundary condition on the body in Eq. (25).

The gradients for the shape parameters are now available as

$$\begin{aligned}\frac{\mathrm{d}\mathscr{L}}{\mathrm{d}\mathbf{a}}=&\frac{\partial}{\partial\mathbf{a}}\left\{\int_{\mathsf{B}(\mathbf{a})}\left[\mathscr{F}(\phi)-\psi\left(\frac{\partial\phi}{\partial z}-w_\alpha\right)\right.\right.\\&\left.\left.+\psi\left(\frac{\partial\phi}{\partial z}-k\phi\right)\right]\mathrm{d}S\right\}\\=&\frac{\partial}{\partial\mathbf{a}}\left\{\int_{\mathsf{B}(\mathbf{a})}[\mathscr{F}(\phi)+\psi w_\alpha-k\psi\phi]\,\mathrm{d}S\right\}.\end{aligned} \tag{29}$$

If the objective is to maximize the damping coefficient, then $\mathscr{F}(\phi)=-\omega\rho w_\alpha\,\mathrm{Im}\,\phi$ and the boundary condition on B becomes

$$\frac{\partial\psi}{\partial z}=\frac{\partial\mathscr{F}}{\partial\phi}=\mathrm{j}\omega\rho w_\alpha.$$

Note that this is a scalar multiple of the boundary condition in Eq. (5) for the original problem. Hence, we conclude that the solution of the adjoint problem is

$$\psi(\mathbf{r})=\mathrm{j}\omega\rho\phi(\mathbf{r}),\quad\mathbf{r}\in\mathsf{V},$$

which satisfies Eqs. (24)–(28). Taking real and imaginary parts gives

$$\mathrm{Re}\,\psi=-\omega\rho\,\mathrm{Im}\,\phi,\quad\mathrm{Im}\,\psi=\omega\rho\,\mathrm{Re}\,\phi. \tag{30}$$

Since $\mathscr{L}$ and $\mathbf{a}$ are real, the derivative in Eq. (29) is real. Hence, we may take its real part. Using the results in Eq. (30) in conjunction with Eq. (29) gives

$$\frac{\mathrm{d}\mathscr{L}}{\mathrm{d}\mathbf{a}}=2\omega\rho\frac{\partial}{\partial\mathbf{a}}\left[\int_{\mathsf{B}(\mathbf{a})}(k\,\mathrm{Im}\,\phi\,\mathrm{Re}\,\phi-\mathrm{Im}\,\phi w_\alpha)\,\mathrm{d}S\right]. \tag{31}$$

The partial derivatives are easily evaluated given the description for the boundary of B in Eq. (22).

Consider the spherical harmonic expansion in Eq. (14) for $\phi=\widetilde{\phi}$ when $R=r$ and $\theta=\pi/2$, i.e., $z=0$. It is clear that if we restrict ourselves to heaving motions, i.e., $w_\alpha=1$, then the integrand of Eq. (31) contains terms of the form $r^M g(\chi)$. Hence, the partial derivatives are constructed as follows:

$$\begin{aligned}\frac{\partial}{\partial a_n}\int_{\mathsf{B}(\mathbf{a})}r^M g(\chi)\,\mathrm{d}S&=\frac{\partial}{\partial a_n}\int_0^{2\pi}\int_0^{r(\mathbf{a},\chi)}r^{M+1}g(\chi)\,\mathrm{d}r\,\mathrm{d}\chi\\&=\frac{\partial}{\partial a_n}\int_0^{2\pi}\frac{1}{M+2}r(\mathbf{a},\chi)^{M+2}g(\chi)\,\mathrm{d}\chi\\&=\int_0^{2\pi}r(\mathbf{a},\chi)^{M+1}\frac{\partial r(\mathbf{a},\chi)}{\partial a_n}g(\chi)\,\mathrm{d}\chi,\end{aligned}$$

where the boundary of B has been described using Eq. (22).

5. Numerical example

At the outset, it should be emphasized that we impose a unit area constraint on the plate structure, i.e.,

using Eq. (22),

$$A = \int_{\mathrm{B}(\mathbf{a})} \mathrm{d}S = \frac{a_0^2}{4} + \sum_{n=1}^{N} \frac{a_n^2}{2} = 1\,\mathrm{m}^2 \tag{32}$$

and $a = \sqrt{A} = 1\,\mathrm{m}$. In implementing the variational solution, the enclosing hemisphere has a radius of $a_h = 1.25 r_{\max}$ where $r_{\max} = \max_\chi r(\mathbf{a}, \chi)$ is the maximum radial dimension of the plate. This choice is based on the results of Damaren (2001) where it was determined that $a_h = 1.25 a_d$ was best for a circular disc of radius a_d and $a_h = \sqrt{a_p^2 + b_p^2}$ was best for a rectangular plate of dimensions $2a_p \times 2b_p$, i.e., circumscribing. The optimal choice was made on the basis of comparison with other published results (i.e., (Miles, 1987) for the disk) and the consistency of identities such as the Haskind relations and the relationship between damping coefficients (calculated using a body integral and the spherical harmonic expansion) and far-field wave amplitudes (calculated using the panel solution on the hemisphere). In general, smaller enclosing hemispheres were better than larger ones at predicting higher frequency damping coefficients. However, the variational method, in general, only produces accurate results in the range $0 \leqslant ka \leqslant 10$.

The hemisphere is paneled with a 40 (circumferential) × 12 (radial) array of panels with angular dimensions of $\Delta\chi = 2\pi/40$ and $\Delta\theta = \pi/24$. For the spherical harmonic expansion in Eq. (14), $M_s = 16$ and $N_s = 20$ which leads to a total (including source panels) of 901 degrees of freedom. The calculated damping coefficient will be nondimensionalized according to $\widehat{\mathscr{J}} = \mathscr{J}/(\omega\rho A a)$.

The values of the damping coefficient are shown in Fig. 3 for a circular plate and a square plate with the same area. In the square case, $N = 40$ Fourier coefficients have been used. Despite the very different nature of the planform shape, the damping coefficients are quite similar. The values given here for a circular disc are in good agreement with those presented by Damaren (2001) which agree with those of Miles (1987) and Martin and Farina (1997). Note that both shapes exhibit a maximum value of $\mathscr{J}$ at a wavenumber of $ka = 1.4$. The close agreement between the damping coefficient of equal-area circular and square plates at $ka = 1.4$ is best understood in terms of the far-field wave behavior: the shape of the outgoing cylindrical wave produced by time-harmonic heaving motions is of very similar shape in both cases.

Let $\mathbf{a}_\mathrm{c}$ denote the Fourier coefficients for the circular plate ($a_0 = 2/\sqrt{\pi}$, $a_n = 0, n \geqslant 1$) and $\mathbf{a}_\mathrm{s}$ denote those for the square plate. We can construct a plate that continuously changes shape from the circular to square case. Its Fourier coefficients are given by

$$\mathbf{a} = [(1-\alpha)\mathbf{a}_\mathrm{c} + \alpha\mathbf{a}_\mathrm{s}]/C_\alpha,$$

where C_α is a normalization factor that enforces unit area. For $\alpha = 0$ we obtain the circular plate whereas for $\alpha = 1$ the square plate is obtained. The damping coefficient is shown in Fig. 4 as a function of α.

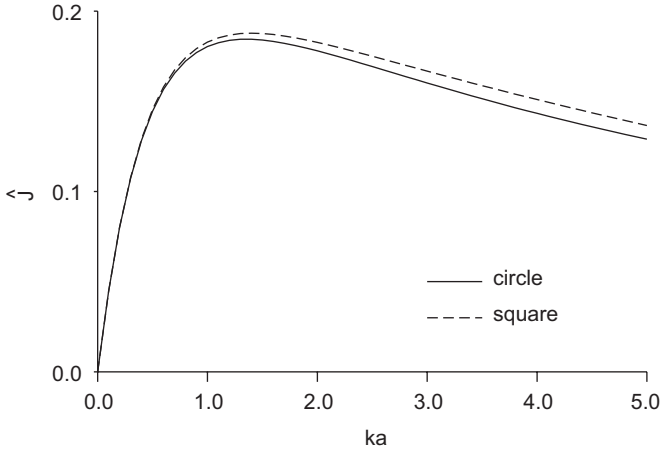

Fig. 3. Damping coefficient vs. wave number for circular and square plates.

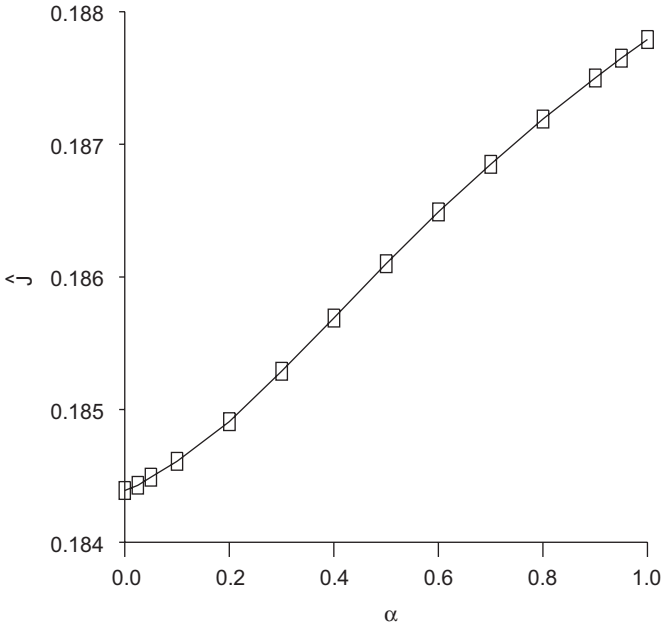

Fig. 4. Damping coefficient vs. morphing parameter.

In an effort to illustrate the matching capabilities of the Chen and Mei variational principle, let us consider the following error measure:

$$E = \|\widetilde{\phi} - \bar{\phi}\|_2 / \|\widetilde{\phi}\|_2, \quad \|\widetilde{\phi}\|_2 = \sqrt{\int_\mathrm{S} \widetilde{\phi}^2 \,\mathrm{d}S}$$

with a similar expression for the matching error in the normal derivative. Both error measures are shown in Fig. 5 for the square plate case as a function of wave number for $0 \leqslant ka \leqslant 5$. The matching which is obtained as a natural boundary condition is enforced within 5%.

For the duration of the study, $ka = 1.4$. Let us consider the gradients produced by the adjoint method in Eq. (31). They will be nondimensionalized according to

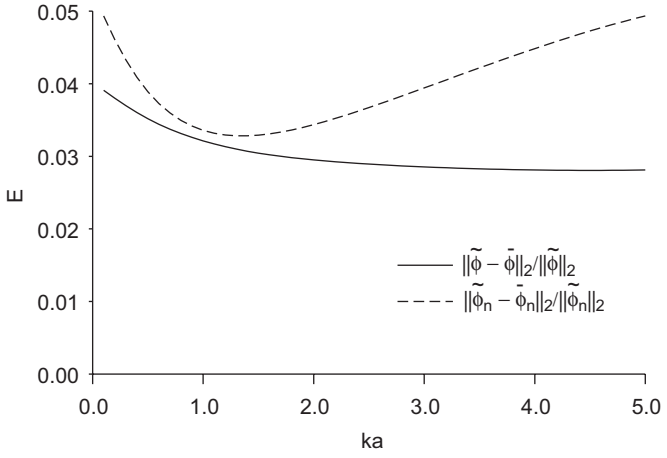

Fig. 5. Matching errors vs. wave number for square plate.

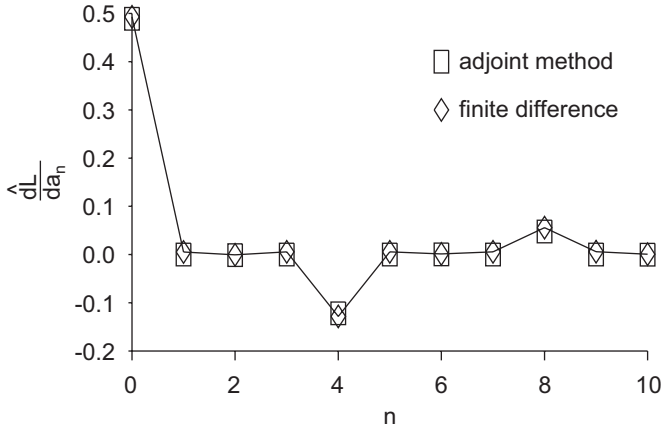

Fig. 6. Adjoint and finite difference gradients (square plate).

$\widehat{d\mathscr{L}}/d\mathbf{a} = d\mathscr{L}/d\mathbf{a}/(\omega\rho A)$. As an independent (but less accurate) check on the results, they can be compared with gradients obtained using finite differences. For this latter calculation, a forward difference is used with a step-size of $\Delta a_n = 0.01$. The adjoint calculation is compared with those obtained using finite differences in Fig. 6 for the case of a square plate approximated with $N = 10$ Fourier terms. Good agreement is obtained but it must be realized that the finite difference calculation is prone to subtractive cancellation errors and approximation errors due to the relatively large step-size. A similar comparison is made in Fig. 7 for the case of the optimal plate shape obtained with $N = 10$ which is described below.

We now consider the shape optimization problem using the optimization code NPSOL. We seek to maximize $\mathscr{J}(\mathbf{a})$ in Eq. (11) subject to the area constraint in Eq. (32). In addition, a perimeter constraint is imposed:

$$P = \int_0^{2\pi} \left[\sqrt{r^2(\mathbf{a},\chi) + \left(\frac{dr}{d\chi}\right)^2} \right] d\chi \leqslant 10\,\mathrm{m}.$$

It was found that this perimeter constraint improved the convergence of the optimization algorithm for $N \geqslant 8$. It is

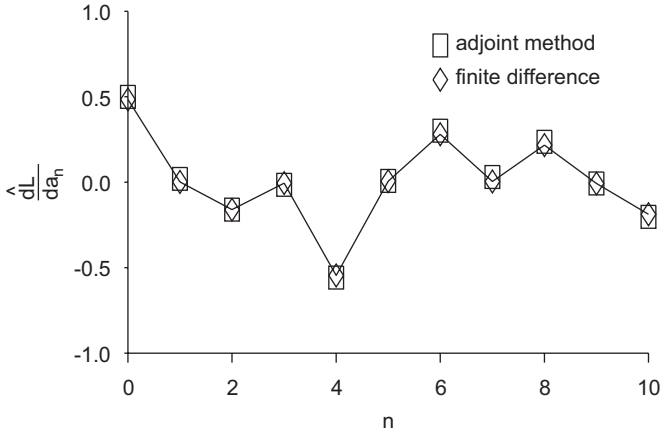

Fig. 7. Adjoint and finite difference gradients (optimal plate).

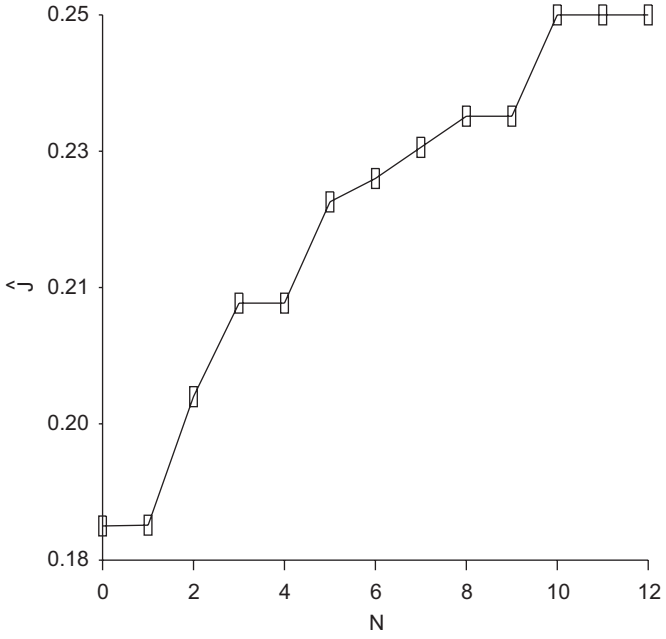

Fig. 8. Optimal damping coefficient vs. number of shape parameters.

also of engineering interest to minimize the shoreline dimension for a structure representative of a floating airport. Also, the radial dimension of the boundary at 360 equally spaced value of χ is constrained not to be below a minimum value:

$$r(\mathbf{a},\chi_i) \geqslant 0.1\,\mathrm{m}, \quad \chi_i = 2\pi i/360, \quad i = 1,\ldots,360.$$

We consider a series of problems with N sequentially increased from $N = 1$ to 12. Note that for $N = 0$, the area constraint uniquely determines a_0. In each case, a circular plate is used as an initial guess for the shape parameters.

The optimal value of $\widehat{\mathscr{J}}$ is shown in Fig. 8 as a function of N. This is, and must be, monotonically increasing since the solution for problem $N-1$ is admissible in problem N. In some cases, there is little or no increase in the performance index. The perimeter constraint was not active for $N \leqslant 7$. We hypothesize that it is impossible for

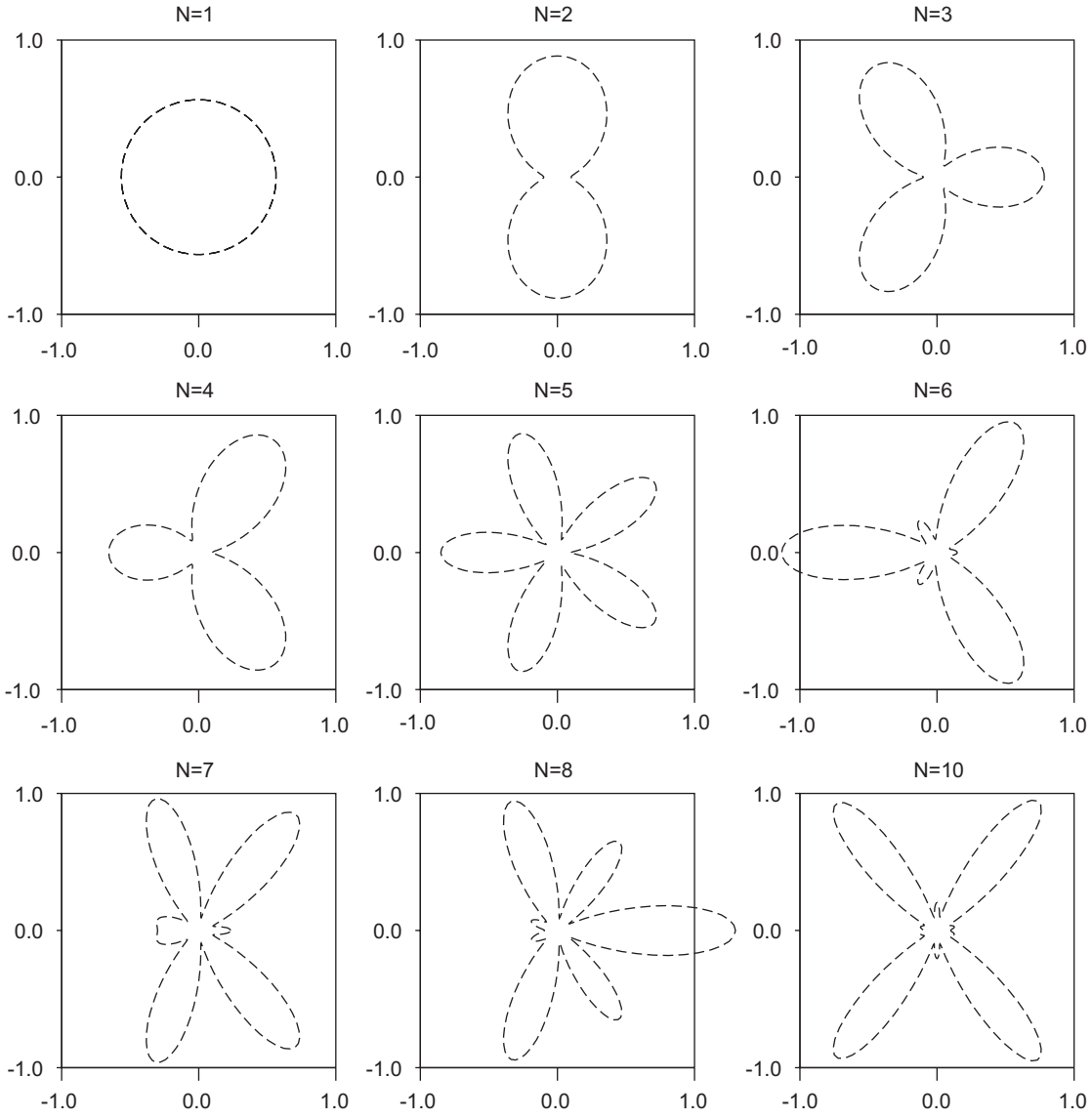

Fig. 9. Optimal plate shapes vs. number of shape parameters.

Table 1
Optimal Fourier coefficients for $N = 10$

n	a_n
0	0.8305
1	0.0012
2	−0.1335
3	−0.0044
4	−0.4263
5	0.0064
6	0.2171
7	0.0028
8	0.1631
9	−0.0059
10	−0.1356

a curve described by Eq. (22) with $N \leqslant 7$ to enclose unit area and have a perimeter as large as 10. This is obvious when $N = 0$. The optimal plate shapes for each problem for $N = 1, \ldots, 10$ (excluding $N = 9$ which is very similar to $N = 8$) are shown in Fig. 9. The optimal values of the a_n for $N = 10$ are given in Table 1. It is this case whose gradients are depicted in Fig. 7. With a little imagination, one can envisage this shape as suitable for a floating airport given the presence of high aspect ratio lobes which are ideal for runway location. It is interesting to note that the replacement of a unit-area circular dock with the optimal shape for $N = 10$ only improves the damping coefficient at $ka = 1.4$ by 35%.

6. Conclusions

A methodology for optimizing the shape of floating plates to maximize added damping in heave at a given wavenumber has been advanced. The flow problem was solved using a previously developed implementation of the Chen and Mei variational principle where an outer field

obtained by distributing sources on an enclosing hemisphere is matched to the field inside the hemisphere described using spherical harmonics. This analytical representation for the field on the body was instrumental in being able to accurately calculate the performance index and its gradients with respect to the shape parameters. The gradients were accurately determined through the development of an adjoint potential flow problem. Somewhat surprisingly, the potential solution of the adjoint problem collapsed down to a scalar multiple of that of the original flow problem. Derivatives with respect to the shape parameters were easily performed given that a Fourier series was used to represent the plate shape.

Future work will address the problem of optimizing radiation damping in the vibration modes of floating plates. This is necessarily more complicated since modification of the shape requires remeshing of a finite element discretization and the vibration modeshapes become shape dependent.

References

Andrianov, A.I., Hermans, A.J., 2005. Hydroelasticity of a circular plate on water of finite or infinite depth. Journal of Fluids and Structures 20, 719–733.

Chen, H.S., Mei, C.C., 1974. Oscillations and wave forces in a man-made harbour in the open sea. In: Tenth Symposium on Naval Research, Office of Naval Research, pp. 573–594.

Clauss, G.F., Birk, L., 1996. Hydrodynamic shape optimization of large offshore structures. Applied Ocean Research 18, 157–171.

Damaren, C.J., 2001. The hydrodynamics of thin floating plates. Ocean Engineering 28, 1145–1170.

Gill, P.E., Murray, W., Saunders, M.A., Wright, M.H., 1998. User's guide for NPSOL 5.0: a fortran package for nonlinear programming. Technical Report SOL 86-1, Systems Optimization Laboratory, Stanford University.

Hulme, A., 1982. The wave forces acting on a floating hemisphere undergoing forced periodic oscillations. Journal of Fluid Mechanics 121, 443–463.

Jameson, A., 1988. Aerodynamic design via control theory. Journal of Scientific Computing 3, 233–260.

Martin, P.A., Farina, L., 1997. Radiation of water waves by a heaving submerged horizontal disc. Journal of Fluid Mechanics 337, 365–379.

Mei, C.C., 1989. The Applied Dynamics of Ocean Surface Waves, second ed. World Scientific, Singapore.

Miles, J.W., 1987. On surface-wave forcing by a circular disk. Journal of Fluid Mechanics 175, 97–108.

Nemec, M., Zingg, D.W., Pulliam, T.H., 2004. Multipoint and multi-objective aerodynamic shape optimization. AIAA Journal 42, 1057–1065.

Newman, J.N., 1984. Double-precision evaluation of the oscillatory source potential. Journal of Ship Research 28, 151–154.

Ragab, S.A., 2001. An adjoint formulation for shape optimization in free-surface potential flow. Journal of Ship Research 45, 269–278.

Ragab, S.A., 2004. Shape optimization of surface ships in potential flow using an adjoint formulation. AIAA Journal 42, 296–304.

Ursell, F., 1981. Irregular frequencies and the motion of floating bodies. Journal of Fluid Mechanics 105, 143–156.

Watanabe, E., Utsunomiya, T., Wang, C.M., 2004. Hydroelastic analysis of pontoon-type VLFS: a literature survey. Engineering Structures 26, 245–256.

Yeung, R.W., 1982. The transient heaving motion of floating cylinders. Journal of Engineering Mathematics 16, 97–119.